

Article

Enhanced Performance of Single-Walled Carbon Nanotube-Germanium Near-Infrared Photodetector by Doping with Au Nanoparticles

Tao Qi ^{1,2}, Yaolun Yu ², Junku Liu ², Yi Jia ² and Dazhi Ding ^{1,*}

¹ Department of Communication Engineering, Nanjing University of Science and Technology, Nanjing 210094, China

² Qian Xuesen Laboratory of Space Technology, China Academy of Space Technology, Beijing 100094, China

* Correspondence: dzding@njjust.edu.cn

Abstract: This paper presents a near-infrared (near-IR) photodetector based on a gold nanoparticles-doped (AuNPs-doped), single-walled carbon nanotube–germanium (SWCNT/Ge) heterojunction. The responsivity, detectivity, and response time of the AuNPs-doped, SWCNT/Ge heterojunction photodetector measured 476 mA W^{-1} (a 291% improvement), $1.0 \times 10^{12} \text{ cm Hz}^{1/2} \text{ W}^{-1}$ (a 208% improvement), and $8 \text{ }\mu\text{s}$, respectively. The mechanism of the enhanced performance originated from the surface modification by gold doping, which effectively improved the work function of the carbon nanotube films and thus increased the barrier height between the heterojunctions, as measured by the contact potential distribution (CPD) and open circuit voltage (V_{oc}) of the SWCNT/Ge interface. In addition, we investigated the effect of various particle sizes on the performance and stability of the photodetector. The results demonstrate the promising prospects of the presented heterojunction photodetector for infrared detection applications.

Keywords: SWCNT/Ge heterojunction; near-infrared photodetector; gold nanoparticles-doped



Citation: Qi, T.; Yu, Y.; Liu, J.; Jia, Y.; Ding, D. Enhanced Performance of Single-Walled Carbon Nanotube-Germanium Near-Infrared Photodetector by Doping with Au Nanoparticles. *Photonics* **2022**, *9*, 615. <https://doi.org/10.3390/photonics9090615>

Received: 18 July 2022

Accepted: 19 August 2022

Published: 30 August 2022

Publisher's Note: MDPI stays neutral with regard to jurisdictional claims in published maps and institutional affiliations.



Copyright: © 2022 by the authors. Licensee MDPI, Basel, Switzerland. This article is an open access article distributed under the terms and conditions of the Creative Commons Attribution (CC BY) license (<https://creativecommons.org/licenses/by/4.0/>).

1. Introduction

The complex and expensive fabrication process of traditional semiconductor detectors limits the development of new infrared photodetectors [1–6]. As an ideal optoelectronic material, carbon nanotubes (CNTs) have unique optical, electrical, thermal, and mechanical properties [7–11], which make them a promising candidate for photoelectric conversion devices, such as photoelectric sensors [12], photodetectors [13], and solar cells [14]. CNTs change the status quo by either forming PN junctions with semiconductor nanomaterials or Schottky junctions with metallic nanomaterials [15–20]. Currently, various carbon nanotube and semiconductor heterostructure photodetectors have been proposed, including CNT–silicon [21], CNT–germanium [22], CNT–gallium arsenide [23], etc. Our former study [22] presented an ozone-treated, SWCNT/Ge heterojunction, near-IR detector. The ozone treatment improved the conductivity of the SWCNT films and formed an oxide layer at the interface, where the responsivity and detectivity were 362 mA W^{-1} and $7.22 \times 10^{11} \text{ cm Hz}^{1/2} \text{ W}^{-1}$, respectively. However, the treated ozone was mainly adsorbed on the surface, and the performance of the SWCNT/Ge photodetector was unstable, so it was necessary to find a better doping method.

Au is a stable metal with a relatively low Fermi level compared with CNTs, so it can be used as a p-type dopant [24–27]. AuNPs can effectively improve the work function and the conductivity of carbon nanotube films [28–32], which enhances the performance of the photodetector. It has been previously demonstrated that by introducing AuNPs on the surface of a CNT photodetector, the photocurrent can be improved by more than three times [33]. Liu et al. [34] exhibited a photodetector based on a AuNPs-modified carbon nanotube with enhanced photodetector responsivity. Chen et al. [35] fabricated a

photodetector composed of a Au nanoparticle/double-walled carbon nanotube film/TiO₂ nanotube array/Ti multilayer heterojunction with a responsivity of 15.41 mA W⁻¹ at a wavelength of 532 nm, which was about 1.91 times higher than the pristine material. Gold nanoparticles are known to locally enhance the incident electromagnetic radiation. These effects are referred to as plasmonic phenomena or plasmonics, and have been suggested for use in photovoltaics to enhance the sensitivity through incident field enhancement; it has also been applied for use in photodetectors; gold nanoparticles in particular have been used to enhance infrared detection [36,37].

In this paper, we report a set of SWCNT/Ge heterojunction photodetectors, deposited with a thin layer of gold nanoparticles through the vacuum evaporation method. Ge, with its bandgap of 0.67 eV, plays a vital role in spectral absorption in the near-infrared region; SWCNT films, with their high conductivity and optical transmittance, serve as a highly conductive network for charge transport and provide a transparent window for light illumination. Due to the favorably improved work function and conductivity of the carbon nanotube film using AuNPs doping, the photovoltaic performance of single-walled carbon nanotube–germanium (SWCNT/Ge) heterojunction photodetectors is greatly enhanced. The responsivity, detectivity, response time, and recovery time of the AuNPs-doped SWCNT/Ge photodetector were 476 mA W⁻¹, 1.0×10^{12} cm Hz^{1/2} W⁻¹, 8 μs, and 8 μs, respectively. These results provide an efficient method for the fabrication of high-performance near-IR photodetectors.

2. Materials and Methods

2.1. SWCNT Film Synthesis and Treatment

Following a floating catalyst chemical vapor deposition process, the SWCNT films were synthesized on a horizontal furnace, using xylene as the carbon source and ferrocene (0.36 mol L⁻¹) and sulfur (0.036 mol L⁻¹) as the catalyst precursors. An automatic syringe pump controlled the carbon source at a feeding rate of 30 μL min⁻¹. After being introduced into the quartz tube, the prepared mixture was transferred to the reaction zone, which had a temperature ranging from 1150 to 1170 °C; the transfer was conducted through a gas mixture of H₂ (400 sccm) and Ar (2000 sccm). The as-prepared SWCNT films were collected by nickel foil and placed at the end of the quartz tube.

2.2. Device Assembly

N-type Ge wafers (2~4 Ω·cm) were soaked in a diluted HF solution to remove the surface oxide layer (GeO₂). The Ge wafers were then washed with deionized water and dried with nitrogen gas. Sellotapes with 0.5 cm internal diameter circuits were cemented to the periphery of the treated Ge wafers to form the insulation layer. Afterwards, the floating SWCNT films on the water surface were transferred onto one of the N-type Ge wafers. Eventually, silver paste was coated between the copper foil and SWCNT films to form an ohmic contact, where the SWCNT films served as the upper electrode. A layer of gold nanoparticles was deposited onto the SWCNT/Ge photodetector surface using a heated thermal evaporator device (TEMDS500, Beijing Technol Science Co., Ltd., Beijing, China) with a vacuum pressure of 2×10^4 Pa and at an evaporation rate of ~ 0.1 Å s⁻¹.

2.3. Characterization

The morphologies of the SWCNT/Ge microstructure were characterized by a scanning electron microscope (SEM, Helios G4 CX, FEI, Hillsboro, OR, USA). The conductivity of a SWCNT film was tested by a digital source meter (2612B, Keithley, OH, USA). The current–voltage (*I*–*V*) characteristics were measured by using a semiconductor device analyzer (B1500A, Keysight, Santa Rosa, CA, USA) with a 1500 nm laser source (25 °C). The contact potential distribution (CPD) of the photodetector was measured by the scanning Kelvin probe microscopy technique (SKPM, cypher VRS, Oxford, OXF, UK).

3. Results

3.1. Characterization of the AuNPs-Doped SWCNT/Ge Photodetectors

The fabrication process of the AuNPs-doped SWCNT/Ge photodetector is shown in Figure 1a. The SWCNT film was transferred to the Ge substrate to form a heterojunction, and AuNPs were deposited on the surface of the SWCNT/Ge photodetector by a heated thermal evaporator device. The surface morphologies of the AuNPs-doped SWCNT/Ge were revealed by the SEM technique (Figure 1b,c). The analysis showed that the deposited AuNPs formed a very compact dense film. As shown in Figure 1d, the statistical particle size distribution showed the morphology of the AuNPs, with an average diameter of ~8 nm and a relatively narrow diameter distribution (ranging from 5 nm to 11 nm). The conductivity of the AuNPs-modified SWCNT films was enhanced by 19.6% compared to the pristine material, as shown in Figure 1e. This result is consistent with the observation from the scanning electron microscopy, where the AuNPs are attached to the CNT films to enhance the conductivity of the carbon nanotube’s network structure.

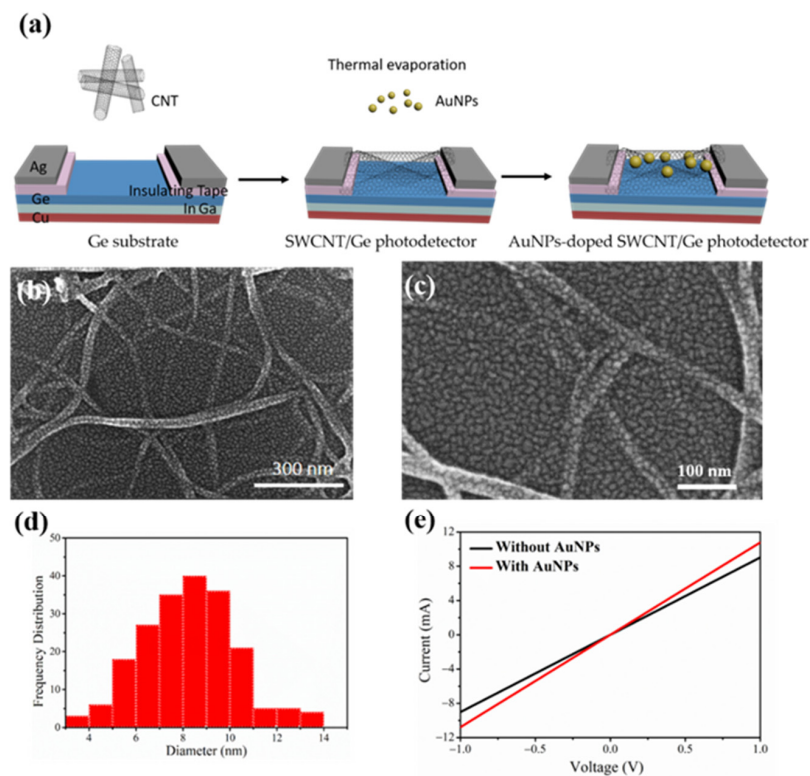


Figure 1. (a): Schematic illustration of the AuNPs-doped SWCNT/Ge photodetector; (b,c): SEM image of the AuNPs-modified SWNT/Ge interface; (d): Statistical particle size distribution of the AuNPs; and (e): I-V curves of the SWNT films with and without gold nanoparticles.

3.2. The Photoelectric Properties of the AuNPs-Doped SWCNT/Ge Photodetectors

Responsivity (R) and detectivity (D^*) are two important parameters to characterize the device quantitatively, and are expressed by the following equations [38]:

$$R = I_p / P_{opt} \tag{1}$$

$$D^* = A^{1/2} R / (2qI_d)^{1/2} = A^{1/2} (I_p / P_{opt}) / (2qI_d)^{1/2} \tag{2}$$

where I_p , P_{opt} , q , A , and I_d are the photocurrent, incident optical power, unit of elementary charge, active detection area, and dark current, respectively. The responsivity measures the sensitivity of the photodetector, while the detectivity of the photodetector represents the ability of detection under weak optical power. The responsivity (R) and detectivity (D^*) were calculated to be 476 mA W^{-1} and $1.0 \times 10^{12} \text{ cm Hz}^{1/2} \text{ W}^{-1}$ under the light power of

0.49 mW, without an external bias voltage. In addition, we observed that the value of the response current was 0.02 mA under the condition of a weak light power of 32 μ W.

$$I_p \propto P_{opt}^\theta \tag{3}$$

Figure 2a shows that the photocurrent increased with the increase of bias voltage. Specifically, the photocurrent increased from 19.5 μ A to 0.75 mA when the optical light power rose from 32 μ W to 3.17 mW. Note that because it is a self-powered photodetector, the photocurrent comes from generating and separating photogenerated carriers without the influence of an external power supply. The photocurrent curve vs. the optical light power, as shown in Figure 2b, can be fitted with Equation (3). The fitted result of the θ is 0.81, and the photogenerated current was nearly proportional to the optical light power. The transient response of the CNT/Ge photodetector was assessed under a 1 Hz light pulsed illumination at zero voltage. As exhibited in Figure 2c, the device’s on and off currents were estimated to be 0.75 mA and 0.14 μ A in the switching state, yielding an on–off ratio as high as 5.4×10^3 .

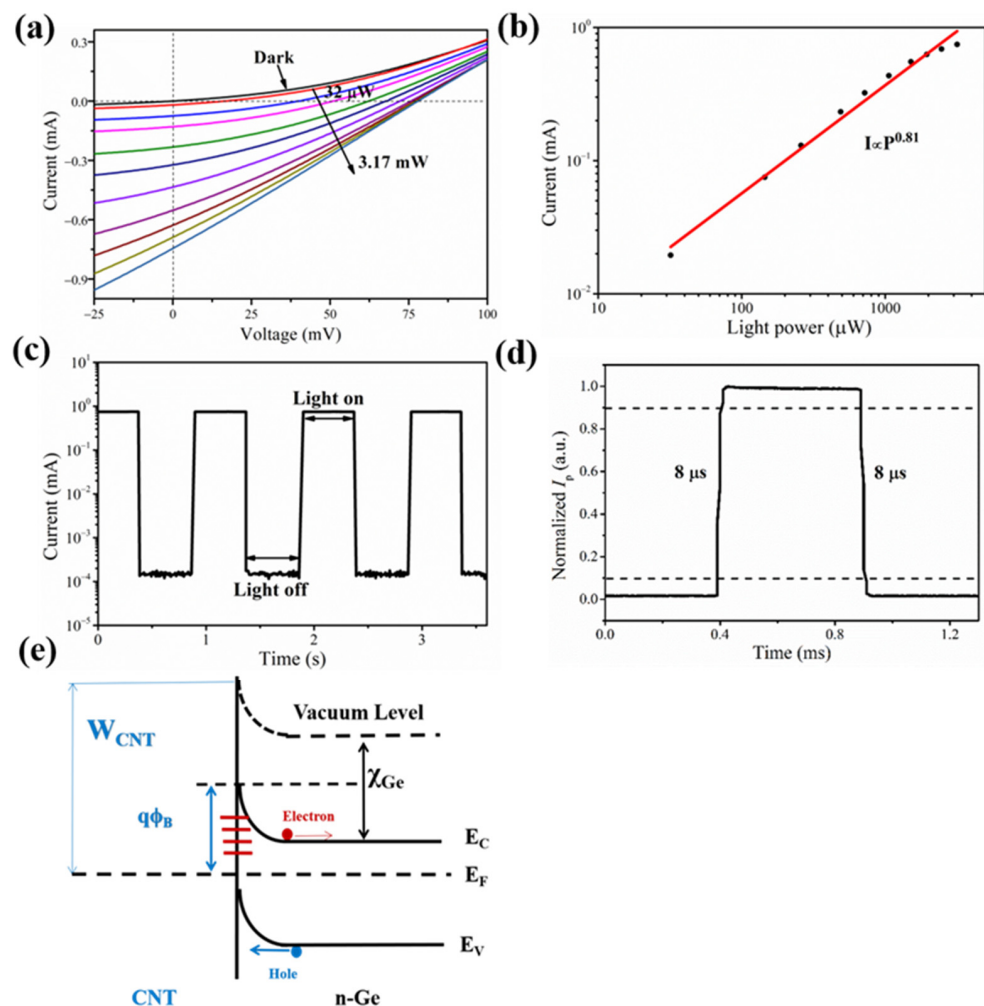


Figure 2. (a) The incident photovoltaic characteristics of the AuNPs-modified SWCNT/Ge photodetector with a gradually increasing light power from 32 μ W to 2.37 mW. (b) The fitting curve between the photogenerated current and the optical power under a 1550 nm light illumination. (c) The turned on and off photo responses of the AuNPs-modified SWCNT/Ge photodetector without an external power supply under a 1550 nm illumination. (d) The normalized cycle measurement at 1 kHz for the response time (τ_r) and recovery time (τ_f). (e) The energy band schematic of the AuNPs-modified SWCNT/Ge photodetector.

Figure 2d shows a single cycle of the photo response under a 1 kHz light illumination, where the rise time (τ_r , increasing from 10% to 90% of the peak value) and fall time (τ_f , decaying from 90% to 10% of the peak value) were estimated to be 8 μ s and 8 μ s, respectively. These results show that the AuNPs-modified SWCNT/Ge photodetector is effective and rapidly separates the photogenerated carriers by forming an efficient Schottky junction.

The $\ln J-V$ characteristics of the SWCNT/Ge heterojunction can be described by the thermionic emission diode equation [39]:

$$J = J_s [\exp (qV/\eta KT) - 1] \tag{4}$$

$$J_s = A^*T^2 \exp (-q\Phi_B/KT) \tag{5}$$

$$\Phi_B = W_{CNT} - \chi_{Ge} \tag{6}$$

where J_s is the reversed saturated current density across the interface, A^* is the effective Richardson constant ($\approx 66 \text{ A K}^{-2} \text{ cm}^{-2}$ for N-type Ge) [40], V is the applied voltage, η is the ideality factor, k is the Boltzmann constant, and T is the absolute temperature. According to these equations, Φ_B can be estimated from the linear fit of the $\ln J-V$ plot. The saturated current density of AuNPs-doped SWCNT/Ge photodetector was estimated to be $\sim 0.196 \text{ mA}$, while Φ_B was calculated to be $\sim 0.62 \text{ V}$. Equation (6) represents the relationship between the work function of the CNT (W_{CNT}) and the electron affinity energy (χ_{Ge}) of Ge. Figure 2e shows the energy band diagrams of the AuNPs-modified SWCNT/Ge heterojunction, where the Schottky junction was formed at the interface of the SWCNT films and N-type Ge. After the AuNPs doping, the increased work function of the carbon nanotube film enhanced the built-in electric field of the SWCNT/Ge junction, which facilitated the separation of photogenerated electron-hole pairs.

3.3. Enhancing the Photoelectric Properties of the SWCNT/Ge Photodetectors with AuNPs Doping

To investigate the effect of the AuNPs modification on the photodetector, Figure 3a shows the $I-V$ curves of SWCNT/Ge photodetector before and after AuNPs modification, revealing the prominent photovoltaic characteristics of the AuNPs-modified SWCNT/Ge junction. After AuNPs deposition, the J_{SC} of the SWCNT/Ge photodetector significantly enhanced from 0.081 mA to 0.23 mA under a 0.49 mW light power illumination, while the V_{oc} of the SWCNT/Ge photodetector increased from 41 mV to 62 mV. Figure 3b shows the V_{oc} of AuNPs-decorated SWCNT/Ge device, which also largely improved and reached 78 mV under the illumination of 3.17 mW light power. The spectral response of the SWCNT/Ge photodetector is shown in Figure 3c. After covering with AuNPs, there was a large enhancement of the optical response in a spectral range from 1250 nm to 2000 nm; this enhancement can be attributed to the fact that AuNPs improve the work function and surface plasmon resonance.

3.4. CPD Measurement before and after AuNPs Modification

The effect of Au nanoparticle doping on the surface potential of the SWCNT/Ge interface was characterized by the SKPM analysis, which measured the strength of the electrostatic forces between a conductive probe and the device. Figure 4a shows that an obvious interface between the Ge and CNT was observed due to the different work functions of the Ge and CNT. Figure 4b shows the pixel-wise histogram distributions of the SWCNT/Ge surface potential, and Figure 4c exhibits the CPD of the SWCNT/Ge heterojunction. The distinction of the work function between the CNT and Ge was obtained using the following equations [40]:

$$eP_{CNT} = W_{tip} - W_{CNT} \tag{7}$$

$$eP_{Ge} = W_{tip} - W_{Ge} \tag{8}$$

$$W_{CNT} - W_{Ge} = eP_{Ge} - eP_{CNT} \tag{9}$$

where W_{Ge} , W_{CNT} , and W_{tip} are the work functions of the Ge, CNT, and conductive probe, respectively; e is the electronic charge, P_{CNT} is the surface CPD between the SKPM probe tip and CNT, and P_{Ge} is the surface CPD between the SKPM probe tip and Ge, respectively. The potential distribution of the CNT and Ge was ~ 720 mV and ~ 870 mV, with a potential difference of ~ 150 mV. Figure 4d shows the potential difference (~ 180 mV) of the SWCNT/Ge heterojunction after AuNPs deposition, and the CPD between SWCNT and Ge increased the number by approximately 30 mV. The above result is consistent with the change in contact with the V_{oc} (which increased by ~ 27 mV).

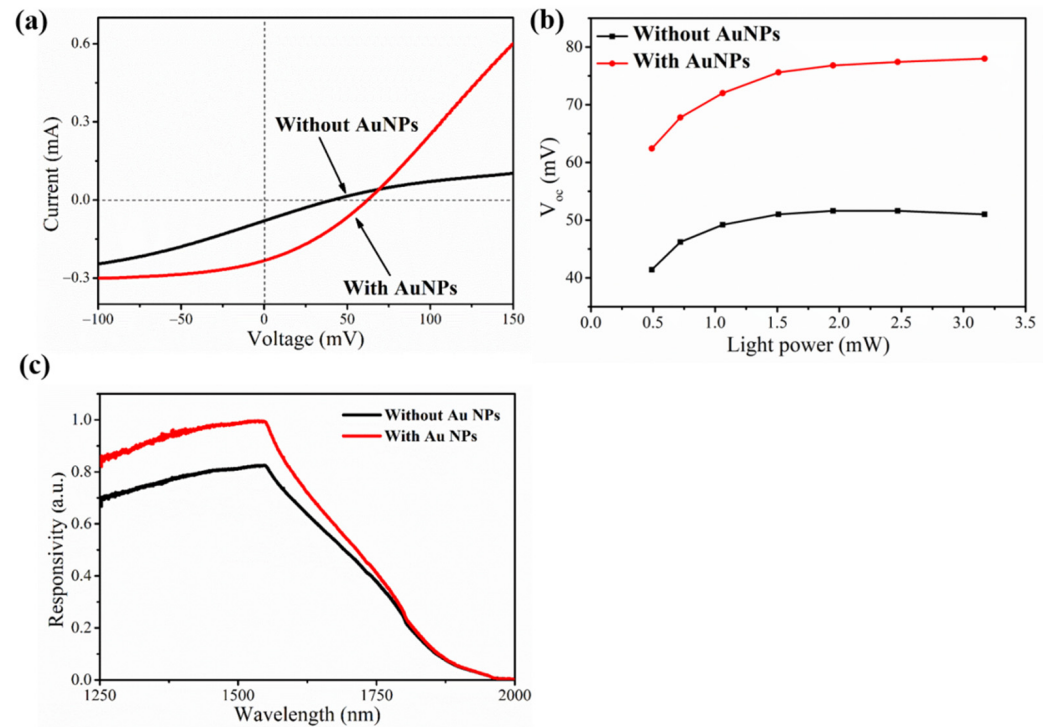


Figure 3. The comparison of the pristine material and the AuNPs-covered SWCNT/Ge photodetector under 0.49 mW light power at a wavelength of 1550 nm. (a) I – V curve of the SWCNT/Ge photodetector. (b) The V_{oc} of the SWCNT/Ge photodetector as a function of the incident light illumination power, which ranged from 0.49 mW to 3.17 mW. (c) Spectral response of SWCNT/Ge photodetector with and without AuNPs.

3.5. The Doping Effect of Particle Size and Stability of the AuNPs SWCNT/Ge

Figure 5a demonstrates that the size of AuNPs dramatically affects the SWCNT/Ge photodetector performance. The responsivity of the SWCNT/Ge heterojunction was enhanced ~ 2.91 times with AuNPs at the size of ~ 8 nm. The doping effect became more significant as the thickness of the Au layer increased with larger Au nanoparticle sizes and higher surface coverage, resulting in an improved responsivity of the SWCNT/Ge photodetector. However, introducing excess AuNPs also led to a decrease in transmittance as the thickness increased. Therefore, the size and coverage of the AuNPs on the SWCNT are vital for obtaining an excellent photodetector performance. Figure 5b compares the stability of the SWCNT/Ge photodetector with ozone and AuNPs doping. We observed that the responsivity of the ozone-treated SWCNT/Ge photodetector declined from 349 mA W^{-1} to 192 mA W^{-1} (decreasing by 45%) after one week, while the responsivity of the AuNPs-doped SWCNT/Ge photodetector only decreased by 10% relative to the original device and obtained a more stable performance one week later. Due to the non-volatile dopant that are AuNPs, the SWCNT/Ge photodetector exhibited a higher stability than with ozone molecule treatment.

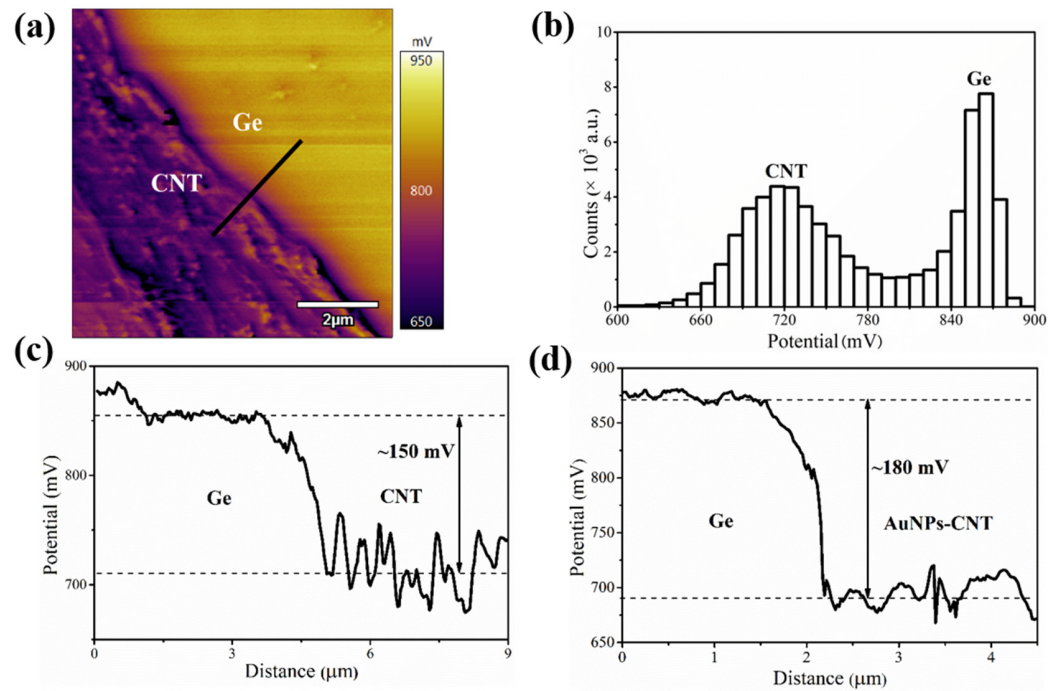


Figure 4. The surface potential of the SWCNT/Ge heterojunction before and after AuNPs modification. (a) The SKPM measurements of the surface potential distribution for the SWCNT/Ge heterojunction. (b) Pixel-wise histogram of the surface potential distribution measurements for the SWCNT/Ge heterojunction. The CPD of (c) the pristine and (d) the AuNPs-modified SWCNT/Ge heterojunction.

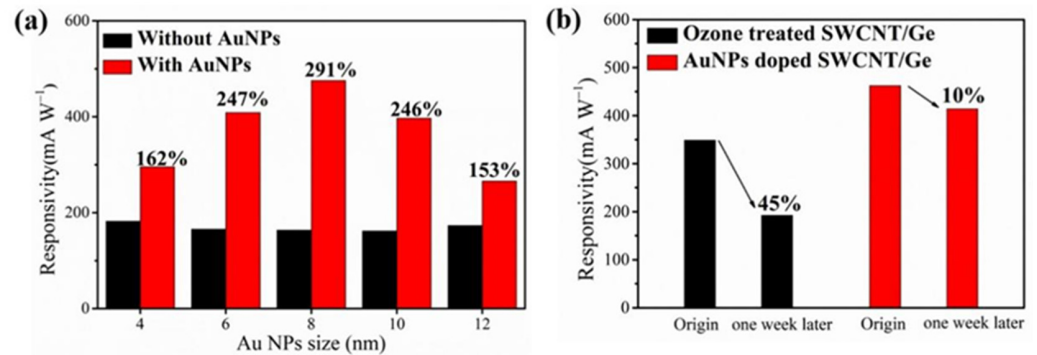


Figure 5. The doping effect of particle size and stability of the AuNPs-doped SWCNT/Ge photodetector. (a) The comparison of the responsivity of the SWCNT/Ge photodetector before and after deposition with various AuNPs particle sizes. (b) Stability of the Au-doped and ozone-treated SWCNT/Ge photodetector.

4. Conclusions

To summarize, we demonstrated an effective method to improve the SWCNT/Ge photodetector performance by introducing AuNPs. The doped AuNPs not only enhanced the conductivity of the SWCNT films, but also improved the work function of the SWCNT films, which further enhanced the built-in electric field and enhanced the performance of the photodetectors. As a result, the responsivity and detectivity of the AuNPs-modified SWCNT/Ge photodetector were estimated to be 476 mA W⁻¹ (increased by 291%) and 1.0 × 10¹² cm Hz^{1/2} W⁻¹ (increased by 208%), respectively. The results revealed that the AuNPs-doped SWCNT/Ge photodetector holds great potential in the emerging optoelectronic applications.

Author Contributions: D.D., Y.J. and Y.Y. designed the project and guided the research; T.Q. and J.L. prepared the test samples and performed the experiments and data analysis; T.Q. wrote the manuscript; Y.J. and Y.Y. reviewed the manuscript. All authors have read and agreed to the published version of the manuscript.

Funding: This work was supported in part by the Natural Science Foundation (Grant No. 62025109 and 61871228) and funded by the Primary Research & Development Plan of Jiangsu Province (Grant No. BE2022070 and BE2022070-1).

Institutional Review Board Statement: Not applicable.

Informed Consent Statement: Not applicable.

Data Availability Statement: Not applicable.

Acknowledgments: The authors thank N. Guo and Y. Hu from the Qian Xuesen Laboratory of Space Technology for their helpful discussions.

Conflicts of Interest: The authors declare no conflict of interest.

References

1. Li, C.; Tian, R.; Yi, R.; Hu, S.; Zhao, J. MoTe₂ PN homojunction constructed on a silicon photonic crystal cavity for high-performance photodetector. *ACS Photonics* **2021**, *8*, 2431–2439. [[CrossRef](#)]
2. Kwon, J.B.; Han, M.; Jung, D.G.; Kong, S.H.; Jung, D. High sensitivity shortwave infrared photodetector based on PbS QDs using P3HT. *Nanomaterials* **2021**, *11*, 2683. [[CrossRef](#)] [[PubMed](#)]
3. Tan, C.; Amani, M.; Zhao, C.; Hettick, M.; Song, X.; Lien, D.H.; Li, H.; Yeh, M.; Shrestha, V.R.; Crozier, K.B. Evaporated Se_xTe_{1-x} thin films with tunable bandgaps for short-wave infrared photodetectors. *Adv. Mater.* **2020**, *32*, 2001329. [[CrossRef](#)] [[PubMed](#)]
4. Balendhran, S.; Hussain, Z.; Shrestha, V.R.; Cadusch, J.; Ye, M.; Sefidmooye Azar, N.; Kim, H.; Ramanathan, R.; Bullock, J.; Javey, A. Copper tetracyanoquinodimethane (CuTCNQ): A metal–organic semiconductor for room-temperature visible to long-wave infrared photodetection. *ACS Appl. Mater. Interfaces* **2021**, *13*, 38544–38552. [[CrossRef](#)]
5. Hou, J.; Wang, Z.; Ding, Z.; Zhang, Z.; Zhang, J. Facile synthesis of VO₂ (M1) nanorods for a low-cost infrared photodetector application. *Sol. Energy Mater. Sol. Cells* **2018**, *176*, 142–149. [[CrossRef](#)]
6. Huang, Z.; Zhang, T.; Liu, J.; Zhang, L.; Jin, Y.; Wang, J.; Jiang, K.; Fan, S.; Li, Q. Amorphous MoS₂ photodetector with ultra-broadband response. *ACS Appl. Electron. Mater.* **2019**, *1*, 1314–1321. [[CrossRef](#)]
7. Gilshteyn, E.P.; Lin, S.; Kondrashov, V.A.; Kopylova, D.S.; Tsapenko, A.P.; Anisimov, A.S.; Hart, A.J.; Zhao, X.; Nasibulin, A.G. A one-step method of hydrogel modification by single-walled carbon nanotubes for highly stretchable and transparent electronics. *ACS Appl. Mater. Interfaces* **2018**, *10*, 28069–28075. [[CrossRef](#)]
8. Xu, W.; Ravichandran, D.; Jambhulkar, S.; Zhu, Y.; Song, K. Hierarchically structured composite fibers for real nanoscale manipulation of carbon nanotubes. *Adv. Funct. Mater.* **2021**, *31*, 2009311. [[CrossRef](#)]
9. Morsi, M.; Rajeh, A.; Al-Muntaser, A. Reinforcement of the optical, thermal and electrical properties of PEO based on MWCNTs/Au hybrid fillers: Nanodielectric materials for organoelectronic devices. *Compos. Part B-Eng.* **2019**, *173*, 106957. [[CrossRef](#)]
10. Oh, Y.; Islam, M.F. Preformed nanoporous carbon nanotube scaffold-based multifunctional polymer composites. *ACS Nano* **2015**, *9*, 4103–4110. [[CrossRef](#)]
11. Hu, Y.; Liu, J.; Chang, L.; Yang, L.; Xu, A.; Qi, K.; Lu, P.; Wu, G.; Chen, W.; Wu, Y. Electrically and sunlight-driven actuator with versatile biomimetic motions based on rolled carbon nanotube bilayer composite. *Adv. Funct. Mater.* **2017**, *27*, 1704388. [[CrossRef](#)]
12. Batista, M.D.R.; Kim, S.J.; Drzal, L.T.; Han, J.-W.; Meyyappan, M. Carbon nanotube-based flexible UV sensor on various substrates. *IEEE Sens. J.* **2020**, *20*, 8429–8436. [[CrossRef](#)]
13. Zhou, H.; Wang, J.; Ji, C.; Liu, X.; Han, J.; Yang, M.; Gou, J.; Xu, J.; Jiang, Y. Polarimetric Vis-NIR photodetector based on self-aligned single-walled carbon nanotubes. *Carbon* **2019**, *143*, 844–850. [[CrossRef](#)]
14. Jeon, I.; Yoon, J.; Kim, U.; Lee, C.; Xiang, R.; Shawky, A.; Xi, J.; Byeon, J.; Lee, H.M.; Choi, M. High-performance solution-processed double-walled carbon nanotube transparent electrode for perovskite solar cells. *Adv. Energy Mater.* **2019**, *9*, 1901204. [[CrossRef](#)]
15. Salvato, M.; Scagliotti, M.; De Crescenzi, M.; Boscardin, M.; Attanasio, C.; Avallone, G.; Cirillo, C.; Proposito, P.; De Matteis, F.; Messi, R. Time response in carbon nanotube/Si based photodetectors. *Sens. Actuators A-Phys.* **2019**, *292*, 71–76. [[CrossRef](#)]
16. Rashid, H.; Sapiee, N.M.; Arsad, N.; Ahmad, H.; Bakar, A.A.A.; Reaz, M.I. Fabrication of a carbon nanotube/tungsten disulfide visible spectrum photodetector. *Appl. Opt.* **2021**, *60*, 2839–2845. [[CrossRef](#)]
17. Salvato, M.; Scagliotti, M.; De Crescenzi, M.; Crivellari, M.; Proposito, P.; Cacciotti, I.; Castrucci, P. Single walled carbon nanotube/Si heterojunctions for high responsivity photodetectors. *Nanotechnology* **2017**, *28*, 435201. [[CrossRef](#)]
18. Yu, T.; Wang, F.; Xu, Y.; Ma, L.; Pi, X.; Yang, D. Graphene coupled with silicon quantum dots for high-performance bulk-silicon-based Schottky-junction photodetectors. *Adv. Mater.* **2016**, *28*, 4912–4919. [[CrossRef](#)]
19. Li, X.; Zhu, M.; Du, M.; Lv, Z.; Zhang, L.; Li, Y.; Yang, Y.; Yang, T.; Li, X.; Wang, K. High detectivity graphene-silicon heterojunction photodetector. *Small* **2016**, *12*, 595–601. [[CrossRef](#)]

20. Huang, Z.; Liu, J.; Zhang, T.; Jin, Y.; Wang, J.; Fan, S.; Li, Q. Interfacial gated graphene photodetector with broadband response. *ACS Appl. Mater. Interfaces* **2021**, *13*, 22796–22805. [[CrossRef](#)]
21. Ong, P.-L.; Euler, W.B.; Levitsky, I.A. Carbon nanotube-Si diode as a detector of mid-infrared illumination. *Appl. Phys. Lett.* **2010**, *96*, 033106. [[CrossRef](#)]
22. Qi, T.; Yu, Y.; Hu, Y.; Li, K.; Guo, N.; Jia, Y. Single-walled carbon nanotube-germanium heterojunction for high-performance near-infrared photodetector. *Nanomaterials* **2022**, *12*, 1258. [[PubMed](#)]
23. Huo, T.; Yin, H.; Zhou, D.; Sun, L.; Tian, T.; Wei, H.; Hu, N.; Yang, Z.; Zhang, Y.; Su, Y. Self-powered broadband photodetector based on single-walled carbon nanotube/GaAs heterojunctions. *ACS Sustain. Chem. Eng.* **2020**, *8*, 15532–15539. [[CrossRef](#)]
24. Kim, S.; Jang, J.; Kim, K.; Park, H.; Bae, J.; Yu, W.; Lee, I.; Kim, G.; Loc, D.; Kim, U. Reduction-controlled viologen in bisolvent as an environmentally stable n-type dopant for carbon nanotubes. *J. Am. Chem. Soc.* **2009**, *131*, 327–331. [[CrossRef](#)] [[PubMed](#)]
25. Kim, S.M.; Jo, Y.W.; Kim, K.K.; Duong, D.L.; Shin, H.-J.; Han, J.H.; Choi, J.-Y.; Kong, J.; Lee, Y.H. Transparent organic P-dopant in carbon nanotubes: Bis (trifluoromethanesulfonyl) imide. *ACS Nano* **2010**, *4*, 6998–7004.
26. Kwon, K.C.; Kim, B.J.; Lee, J.-L.; Kim, S.Y. Effect of anions in Au complexes on doping and degradation of graphene. *J. Mater. Chem. C* **2013**, *1*, 2463–2469. [[CrossRef](#)]
27. Zhang, H.; Xiong, J.; Ye, M.; Li, J.; Zhang, X.; Quhe, R.; Song, Z.; Yang, J.; Zhang, Q.; Shi, B. Interfacial properties of monolayer antimonene devices. *Phys. Rev. Appl.* **2019**, *11*, 064001.
28. Choi, K.; Yu, C. Highly doped carbon nanotubes with gold nanoparticles and their influence on electrical conductivity and thermopower of nanocomposites. *PLoS ONE* **2012**, *7*, e44977.
29. Kong, B.-S.; Jung, D.-H.; Oh, S.-K.; Han, C.-S.; Jung, H.-T. Single-walled carbon nanotube gold nanohybrids: Application in highly effective transparent and conductive films. *J. Phys. Chem. C* **2007**, *111*, 8377–8382.
30. Khoo, K.; Chelikowsky, J.R. Electron transport across carbon nanotube junctions decorated with Au nanoparticles: Density functional calculations. *Phys. Rev. B* **2009**, *79*, 205422.
31. Yang, S.B.; Kong, B.-S.; Geng, J.; Jung, H.-T. Enhanced electrical conductivities of transparent double-walled carbon nanotube network films by post-treatment. *J. Phys. Chem. C* **2009**, *113*, 13658–13663. [[CrossRef](#)]
32. Mao, S.; Lu, G.; Yu, K.; Chen, J. Specific biosensing using carbon nanotubes functionalized with gold nanoparticle–antibody conjugates. *Carbon* **2010**, *48*, 479–486. [[CrossRef](#)]
33. Zhou, C.; Wang, S.; Sun, J.; Wei, N.; Yang, L.; Zhang, Z.; Liao, J.; Peng, L.-M. Plasmonic enhancement of photocurrent in carbon nanotube by Au nanoparticles. *Appl. Phys. Lett.* **2013**, *102*, 103102. [[CrossRef](#)]
34. Liu, J.; He, W.; Hu, L.; Liu, Z.; Zhou, H.; Wu, X.; Sun, L. Visible light detection using single-walled carbon nanotube film and gold nanoparticles or nanorods. *Appl. Phys. Lett.* **2010**, *107*, 094311. [[CrossRef](#)]
35. Chen, Y.; Zhang, G.; Dong, Z.; Wei, J.; Zhu, J.-L.; Sun, J.-L. Fabrication of Au nanoparticle/double-walled carbon nanotube film/TiO₂ nanotube array/Ti heterojunctions with low resistance state for broadband photodetectors. *Phys. B* **2017**, *508*, 1–6. [[CrossRef](#)]
36. Gaponenko, S.V.; Guzatov, D.V. Colloidal plasmonics for active nanophotonics. *Proc. IEEE* **2020**, *108*, 704–720. [[CrossRef](#)]
37. Chen, M.; Shao, L.; Kershaw, S.V. Photocurrent enhancement of HgTe quantum dot photodiodes by plasmonic gold nanorod structures. *ACS Nano* **2014**, *8*, 8208–8216. [[CrossRef](#)]
38. Choi, J.-M.; Jang, H.Y.; Kim, A.R.; Kwon, J.-D.; Cho, B.; Park, M.H.; Kim, Y. Ultra-flexible and rollable 2D-MoS₂/Si heterojunction-based near-infrared photodetector via direct synthesis. *Nanoscale* **2021**, *13*, 672–680. [[CrossRef](#)]
39. Kwon, M.G.; Kim, C.; Chang, K.E.; Yoo, T.J.; Kim, S.-Y.; Hwang, H.J.; Lee, S.; Lee, B.H. Performance enhancement of graphene/Ge near-infrared photodetector by modulating the doping level of graphene. *APL Photonics* **2022**, *7*, 026101. [[CrossRef](#)]
40. Zhao, M.; Zhu, W.; Feng, X.; Yang, S.; Liu, Z.; Tang, S.; Chen, D.; Guo, Q.; Wang, G.; Ding, G. Role of interfacial 2D graphene in high performance 3D graphene/germanium Schottky junction humidity sensors. *J. Phys. Chem. C* **2020**, *8*, 14196–14202. [[CrossRef](#)]